

Surfactant-Mediated Growth of Twisted Bilayer Graphene on SiC

Y.-R. Lin,^{1, 2,*} N. Samiseresht,^{1, 2,*} M. Franke,^{1, 2} S. Parhizkar,^{1, 2} S. Soubatch,^{1, 2}
B. Amorim,³ T.-L. Lee,⁴ C. Kumpf,^{1, 2} F.S. Tautz,^{1, 2} and F.C. Bocquet^{1, 2, †}

¹*Peter Grünberg Institut (PGI-3), Forschungszentrum Jülich, 52425 Jülich, Germany*

²*Jülich Aachen Research Alliance (JARA), Fundamentals of Future Information Technology, 52425 Jülich, Germany*

³*CeFEMA, Instituto Superior Técnico, Universidade de Lisboa, Avenida Rovisco Pais, 1049-001 Lisboa, Portugal*

⁴*Diamond Light Source Ltd, Didcot, OX110DE, Oxfordshire, United Kingdom*

(Dated: June 8, 2022)

We propose a method to grow high-quality twisted bilayer graphene epitaxially on SiC using borazine as a surfactant. With this method, closed layers with a constant orientation with respect to the substrate can be grown over mm-size samples. Using high-resolution electron diffraction, we find a twist angle distribution centered at 30° with a standard deviation of $(0.46 \pm 0.01)^\circ$, a compression of the top (rotated) graphene layer by 0.7% with respect to the bottom layer, and a $(N \times N)R0^\circ$ Moiré unit cell with $N = 12.84 \pm 0.12$ with respect to the top graphene. The interlayer hopping resulting from a comparison of tight binding simulations with angle-resolved photoelectron spectroscopy agrees with values reported for other twist angles.

PACS numbers: 73.22.Pr, 61.48.Gh, 61.05.jh, 79.60.Jv

Since the isolation of the first two-dimensional material, graphene, by micromechanical cleavage of graphite in 2004 [1], efforts have been made to control the electronic properties of graphene without affecting the lattice. Twisted bilayer graphene (tBLG) has already been identified as a promising candidate in 2007 [2]. In this material, the twist angle [3] as well as the relative strain [4–7] between the top and the bottom layers are decisive parameters that determine the electronic properties of the system. Among the intriguing properties of tBLG are chirality [8–10], magnetism [11, 12], and a tunable band gap [13–15]. More recently, this system has attracted additional interest after unconventional superconductivity was discovered for twist angles of approximately 1.1° [16, 17].

Up to now, most experimental studies of tBLG are performed on manually stacked, exfoliated graphene single layers. This method has the advantage that virtually any material can be stacked with any angle, but the moderate material quality, small sample size and limited twist angle control are its major shortcomings. For example, the presence of interlayer contaminants forming bubbles is a challenging issue [18]. Moreover, this method is not scalable. In contrast, epitaxial growth is more limited in scope, but if the correct growth parameters for a given stack and a given twist angle have been identified, it is reproducible and readily scalable, and it offers unrivaled cleanliness and control at the atomic scale.

tBLG can be grown epitaxially on metals. Examples are Pt(111) [19], Pd foil [20], Pd(111) [21], Cu foil [22–24], Ni–Cu gradient foil [25], Ir(111) [26], Ni(111) [27]. Thermal decomposition of 6H-SiC(0001) is another route to obtain tBLG [28–30]. However, in all of these cases one finds random twist angles and/or random orientation across the sample, and each domain of a given twist angle has a typical maximum diameter of 1 to 10 μm .

This makes these samples unsuitable for any application that requires a definite twist angle and orientation with respect to the substrate over a large area. Furthermore, the limited domain size and random orientation make the use of non-local characterization techniques for these samples difficult. For example, measuring the electronic band structure by means of angle-resolved photoemission spectroscopy (ARPES) requires a highly focused photon beam (nano-ARPES) to address only one twist angle at a time [19, 22, 25, 30–32].

In this Letter, we report a method for growing tBLG with a well-defined twist angle and orientation on a macroscopic scale. Specifically, we anneal SiC in a borazine ($\text{B}_3\text{N}_3\text{H}_6$) atmosphere. Thereby, borazine acts as a surface-active molecule (surfactant), enforcing a specific rotation of the top graphene layer. Since the growth of the rotated graphene layer is self-limiting and the growth temperature is below the one required for multilayer non-rotated graphene, only tBLG is formed. As a substrate we use the silicon-terminated 6H-SiC(0001) surface. Because of the very high quality of the obtained tBLG, leading to sharp diffraction spots, it is possible to detect its Moiré, and to accurately determine the azimuthal distribution of twist angles, the average strain and the average domain size for each of the two graphene layers.

Our method is based on two well-known facts. Firstly, it has long been established that on SiC(0001), large single-layer graphene domains can be obtained by annealing the sample in a high pressure argon environment [33, 34]. The same structure can be obtained by growing in ultra-high vacuum (UHV), with only the domains being smaller [33]. The natural lattice orientation of such epitaxial monolayer graphene (EMLG) on SiC(0001) is 30° with respect to the SiC lattice, and its lattice is compressed by 0.22% relative to graphite [35]. Further an-

nealing leads to the growth of a second graphene layer of the same orientation below the initial one. Secondly, it has recently been shown that single-layer hexagonal boron nitride (hBN) grows epitaxially on 6H-SiC(0001) in a borazine atmosphere [36]. The hBN lattice vectors are aligned with the SiC substrate surface lattice vectors (hBN- $R0^\circ$) [56]. By annealing hBN- $R0^\circ$ to higher temperatures, a graphene single layer (SLG- $R0^\circ$) gradually forms in the hBN- $R0^\circ$, following its orientation and finally replacing it [36]. This observation, in conjunction with the well-known fact that multilayer $R30^\circ$ graphene can be grown on SiC by thermal decomposition, suggests that 30° -tBLG may be grown on SiC(0001) with the help of hBN [37]. However, it is clear that in such a scheme, the quality of the final 30° -tBLG is limited by the quality of the formed hBN layer. In order to eliminate this influence, we propose using borazine as a surfactant molecule during the growth of 30° -tBLG, thus avoiding the stabilization of a static hBN lattice but keeping the orienting influence of hBN nuclei which act as a template for the growth of rotated graphene. This dynamic approach may offer the advantage that, because borazine molecules are provided continually during growth, small hBN nuclei are constantly present at the surface until a closed rotated graphene layer is formed. It also avoids the negative effects of domain boundaries in large-scale static hBN, lattice mismatch between graphene and hBN etc. As we show in this Letter, the surfactant-mediated growth indeed provides 30° -tBLG of superior quality.

The SiC wafers were obtained from TankBlue Semiconductor Co. Ltd. The sample, a 5×10 mm 2 N-doped 6H-SiC(0001) wafer piece, is cleaned by annealing in UHV while being exposed to a flux of silicon atoms. In this way, the Si-rich ($\sqrt{3} \times \sqrt{3}$) $R30^\circ$ reconstruction is prepared [39]. The temperature is controlled by direct current heating and measured by a pyrometer [57]. After the cleaning process, we prepare the more Si-rich (3×3) reconstruction [40] and then anneal the sample directly to 1380°C in a partial pressure of borazine (1.5×10^{-6} mbar) to obtain 30° -tBLG. If one carries out the same process at a lower temperature (1225°C), SLG- $R0^\circ$ of poor crystalline quality forms. At an even lower temperature (1100°C) hBN- $R0^\circ$ grows.

All results reported in this Letter were obtained from three different UHV setups. All sample transfers between the setups were performed in UHV using a pumped suitcase. In the first setup, we prepared the samples and characterize them with low energy electron diffraction (LEED) and angle-resolved photoelectron spectroscopy (ARPES) using a monochromatized UV lamp ($h\nu = 21.2$ eV) and a Scienta R4000 analyzer. Quantitative diffraction was performed in a second setup using spot profile analysis LEED (SPA-LEED). In these two setups, the sample was held at room temperature. Finally, ARPES at 105 eV photon energy was performed with a SPECS Phoibos 225 analyzer in an end-station of the

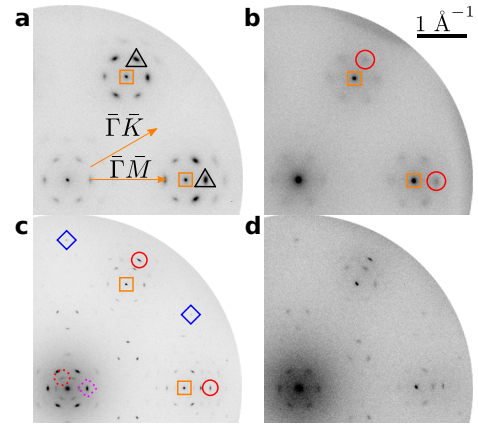


FIG. 1: SPA-LEED patterns of (a) hBN- $R0^\circ$, (b) SLG- $R0^\circ$, (c) 30° -tBLG grown by annealing SiC(0001)-(3 \times 3) in a borazine atmosphere and (d) 30° -tBLG grown by annealing SLG- $R0^\circ$ in UHV. First order diffraction spots are assigned as follows: \square – 6H-SiC(0001); \triangle – hBN- $R0^\circ$; \circ – G- $R0^\circ$; \diamond – G- $R30^\circ$; Dotted diamond – 30° -tBLG Moiré. The dotted circle indicates the well-known apparent (6 \times 6) periodicity of the $(6\sqrt{3} \times 6\sqrt{3})R30^\circ$ buffer layer. The high symmetry directions of the SiC surface Brillouin zone are indicated in (a). All patterns have the same gray scale and were acquired with an impact energy of 165 eV.

I09 beamline at the Diamond Light Source in Didcot, UK, at a sample temperature of 20 K. All used techniques have an electron or photon beam footprint on the sample ranging from 0.05 to 3 mm 2 and thus provide an averaged signal from the sample.

Fig. 1 displays SPA-LEED patterns obtained at various growth stages. Fig. 1(a) shows the diffraction pattern obtained by annealing the SiC(0001)-(3 \times 3) reconstruction to 1100°C in a borazine atmosphere. Around each first order $\langle 10 \rangle$ SiC diffraction spot [58], marked by orange squares (\square), we observe a hexagonal arrangement of elongated diffraction spots. The lattice constant corresponding to the spots marked by black triangles (\triangle) (2.576 ± 0.01) Å agrees with the value reported for single-layer hBN on SiC [36], exhibiting an average tensile strain of 2.84% relative to the hBN bulk lattice parameter of (2.5047 ± 0.0002) Å [41]. The position and elongation of these spots indicate that the hBN domains are aligned to the $\bar{\Gamma}\bar{M}$ direction of SiC within a small but significant azimuthal range. We therefore conclude that, at this annealing temperature, hBN- $R0^\circ$ forms on the SiC surface. The other diffraction spots in Fig. 1(a) are attributed to multiple electron scattering on different lattices. We note that the diffraction pattern of hBN- $R0^\circ$ grown on SiC cannot be recovered after 48 hours air exposure followed by a mild annealing in UHV. As hBN is known to be stable in air [42], our observation suggests that hBN- $R0^\circ$ does not form a closed layer, thus allowing the oxidation of SiC.

Fig. 1(b) shows the diffraction pattern obtained after

annealing hBN- $R0^\circ$ in UHV at 1225°C . The same pattern can alternatively be obtained by annealing SiC(0001)-(3 \times 3) directly to the same temperature in a borazine atmosphere. As for hBN- $R0^\circ$, the diffraction pattern shows a hexagonal arrangement of spots around the $\langle 10 \rangle$ spots of SiC (\square). However, the lattice constant of the spots marked by red circles (\bigcirc) (2.524 ± 0.02 Å) is smaller than the one found for hBN- $R0^\circ$. The presence of Dirac cones at the \bar{K} points of this lattice (not shown) proves that it corresponds to single-layer graphene aligned to the SiC substrate (SLG- $R0^\circ$), in agreement with Ref. [36]. Note that SLG- $R0^\circ$ in Fig. 1(b) has an average tensile strain of 2.55% relative to graphite (2.461 Å [35, 43]). Moreover, the diffraction pattern is characterized by very broad spots with low intensity and high background. This indicates that the graphene domains are small and accompanied by large areas without long-range order, and is consistent with the fact that its diffraction pattern cannot be recovered after 48 hours of air exposure.

Fig. 1(c) displays the diffraction pattern obtained by annealing SiC(0001)-(3 \times 3) directly to 1380°C in a borazine atmosphere. The elongated diffraction spots marked by red circles (\bigcirc) correspond to a lattice parameter of (2.439 ± 0.006) Å, and are assigned to a graphene layer aligned to the SiC substrate (G- $R0^\circ$), as evidenced by the observation of Dirac cones (see below). Additionally, diffraction spots corresponding to a similar lattice parameter, but aligned with $\bar{\Gamma}\bar{K}$ of SiC ($R30^\circ$), are present (\diamond). They originate from a second type of graphene rotated by 30° with respect to the substrate (G- $R30^\circ$). The following two observations suggest that these two graphene layers are stacked, G- $R0^\circ$ on top of G- $R30^\circ$. First, the G- $R30^\circ$ has a smaller intensity than G- $R0^\circ$ – this can be explained by the attenuation of the electron diffraction intensity. Second, unlike G- $R0^\circ$, G- $R30^\circ$ has diffraction spots with a circular shape, which can be understood as a consequence of the rigid locking of the layer to the SiC substrate, yielding superior azimuthal order similar to EMLG [44]. Interestingly, the diffraction pattern of this 30° -tBLG is recovered after four months air exposure and a mild annealing in UHV. This indicates that 30° -tBLG forms a closed layer across the SiC surface.

Fig. 1(d) displays the diffraction pattern obtained by annealing SLG- $R0^\circ$ at 1380°C in UHV, an alternative route reported in Ref. [37] to prepare 30° -tBLG. The pattern is the same as in Fig. 1(c), however, the background intensity is noticeably higher, the spots are much broader and we observe fewer higher-order diffraction spots. We conclude that this preparation method yields a 30° -tBLG with not only lower crystalline quality but also areas without long-range order. In the following, we concentrate exclusively on the high-quality 30° -tBLG in Fig. 1(c).

Deeper insight into the quality of the crystalline structures in Fig. 1(c) is provided by the analysis of the respec-

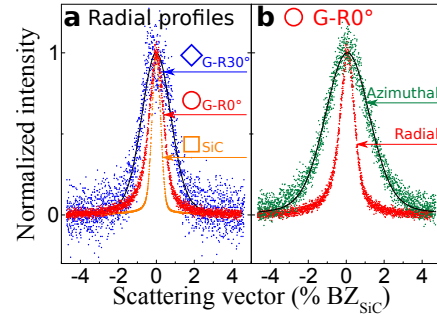


FIG. 2: Electron diffraction spot profiles taken on 30° -tBLG prepared in a borazine atmosphere (see Fig. 1(c)). (a) Typical radial profiles of $\langle 10 \rangle$ spots of G- $R30^\circ$, G- $R0^\circ$ and SiC. (b) Radial and azimuthal profiles of the $\langle 10 \rangle$ spot of G- $R0^\circ$. The profiles have normalized intensity. Colored dots represent experimental data. Black lines are fits (only shown for broad profiles).

tive $\langle 10 \rangle$ diffraction spot profiles (Fig. 2). The full width at half maximum (FWHM) w of the radial spot profile arises from the combined effect of the finite instrumental resolution and the finite size of crystalline domains. $2\pi/w$ represents a lower limit to the average domain size. Moreover, an azimuthal profile broader than the radial profile is a direct indication of azimuthal disorder. To estimate the azimuthal distribution, we convolve radial profile with a Gaussian to fit the azimuthal profile. The standard deviation σ of the fitted Gaussian is a measure of the azimuthal disorder.

Radial $\langle 10 \rangle$ spot profiles are shown in Fig. 2(a). The $\langle 10 \rangle$ SiC spots (\square) have a circular shape and the radial line profile is fitted by a Voigt function with a FWHM of (0.525 ± 0.002) %BZ_{SiC}, or (0.01237 ± 0.00005) Å⁻¹. In real space, this corresponds to an average domain size > 508 Å [59]. Next, we consider the $\langle 10 \rangle$ spots of G- $R30^\circ$ (\diamond). These spots have a circular shape that corresponds to an average domain size > 147 Å. In contrast, the $\langle 10 \rangle$ spots of G- $R0^\circ$ (\bigcirc) are elongated in the azimuthal direction. Its radial profile corresponds to an average domain size > 290 Å, significantly larger than for G- $R30^\circ$. This difference in domain size within the 30° -tBLG layer is explained by the fact that G- $R30^\circ$ can only grow if G- $R0^\circ$ is already present locally, thus protecting the former from borazine. Therefore, the G- $R30^\circ$ domains are necessarily smaller.

It is clear from Fig. 2(b) that the azimuthal profile of the top graphene layer G- $R0^\circ$ is broader than its radial profile. This is evidence that several azimuthal orientations of G- $R0^\circ$ coexist on the surface. We find $\sigma = (0.46 \pm 0.01)^\circ$ around the $R0^\circ$ direction. As the bottom graphene layer has an exact $R30^\circ$ orientation (circular spots), approximately 70% of the 30° -tBLG consists of bilayer graphene with twist angles ranging from 29.54° to 30.46° .

The narrow twist angle distribution in 30° -tBLG

suggests a non-vanishing interaction between the two graphene layers. Additional indications of such an interaction come from a further analysis of the diffraction pattern, yielding two important observations. Firstly, close to $(0,0)$, there are additional spots in Fig. 1(c), one of them marked by a dotted circle, which cannot be explained by either of the two graphene layers (\diamond , \bigcirc), the buffer layer (dotted diamonds) [60], the SiC substrate (\square) or multiple scattering involving those individual lattices. Therefore, they must arise from a Moiré modulation of the complete 30° -tBLG. This corresponds to a $(N \times N)R0^\circ$ lattice with $N = 12.84 \pm 0.12$ with respect to the unit-cell of G- $R0^\circ$, or with $N = 10.17 \pm 0.10$ with respect to SiC. Note that in the case of an electron density modulation forming the Moiré, the structural modulation may even be larger. An analogous effect is well known for EMLG on SiC [44–46]. Secondly, looking at the precise lattice constant of G- $R0^\circ$, we find that it is 0.7% contracted with respect to G- $R30^\circ$. Together with the azimuthal distribution of twist angles, these two observations show that 30° -tBLG grown in borazine atmosphere relaxes locally around the perfect quasicrystalline order of two unstrained 30° -rotated graphene lattices [47], in order to minimize its energy. This might be, at least partially, an effect of the SiC(0001) substrate. A detailed structural investigation requires microscopic real space methods and is beyond the scope of this Letter. Note that in the absence of the SiC substrate and the buffer layer, the structure of minimum energy of 30° -tBLG may differ from the one observed here [37].

We now turn to the electronic properties of our 30° -tBLG sample. An ARPES constant binding energy map (CBM) taken close to the Dirac energies is presented in Fig. 3(a). The intensity found at the \bar{K} points of the individual graphene layers in the CBM of Fig. 3(a) together with the linear band dispersion in the energy distribution maps (EDM) in Fig. 3(b)-(c) demonstrate the presence of two graphene layers with a difference in orientation of approximately 30° . The G- $R30^\circ$ is *n*-doped with $E_D = (0.37 \pm 0.01)$ eV, and G- $R0^\circ$ with $E_D = (0.41 \pm 0.01)$ eV. The intensity at \bar{K}_{0° is approximately six times higher than at \bar{K}_{30° . The absorption of G- $R30^\circ$ photoelectrons by G- $R0^\circ$, and the lower coverage of G- $R30^\circ$ as found in SPA-LEED data, explain this difference [61]. The Dirac cone replicas around \bar{K}_{0° , indicated by red dotted diamonds in Fig. 3(a), arise from the diffraction of photoelectrons from the top G- $R0^\circ$ by the buffer layer lattice located below G- $R30^\circ$, as seen for EMLG [48]. This is the ultimate proof that we have indeed prepared 30° -tBLG. Due to the reduced intensity at \bar{K}_{30° , the replicas around this point (blue dotted diamonds) cannot be detected.

The high quality of our 30° -tBLG sample offers the possibility to search for interlayer coupling in the electronic band structure. If such a coupling is present, one expects the formation of band gaps at the position

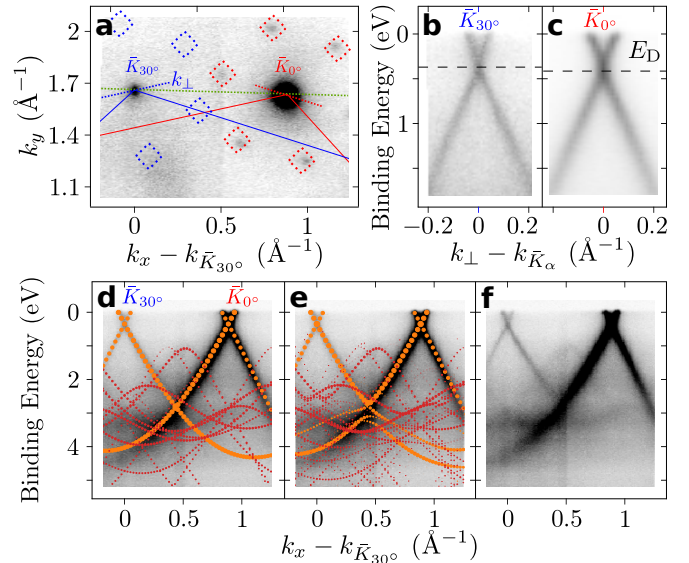


FIG. 3: (a) Experimental CBM of 30° -tBLG, at a binding energy of 0.39 eV, superposed with a zoom of the Brillouin zones of G- $R0^\circ$ (red line) and G- $R30^\circ$ (blue line). The dotted lines indicate where the EDM shown in the following panels are taken. (b) EDM at \bar{K}_{30° in the $\bar{K}_{30^\circ} - \bar{K}_{30^\circ}$ direction, (c) similarly at \bar{K}_{0° . The intensities in panel (b) are multiplied by a factor six in comparison to panel (c) in order to obtain comparable gray scales. (d)-(f) The three identical gray-scale images show the EDM along the $\bar{K}_{30^\circ} - \bar{K}_{0^\circ}$ direction (green dotted line in (a)). The size of the orange dots indicates the simulated ARPES intensity for freestanding 30° -tBLG with (d) $V_{pp\sigma}^0 = 0$ eV and (e) $V_{pp\sigma}^0 = 0.2$ eV (see text). The ARPES intensity induced by the six buffer layer replicas (dotted diamonds in panel (a)) is represented by red dots.

where Dirac cones of the two different layers cross. In Fig. 3(d)-(f), the EDM along the $\bar{K}_{0^\circ} - \bar{K}_{30^\circ}$ direction is shown. The crossing is found midway between the two Dirac cones at a binding energy of approximately 2.7 eV. To interpret our ARPES data, we simulate the electronic band structure within the tight binding approximation and the one-step model of photoemission, using the plane wave approximation for the final state (orange dots) [49] [62]. Despite replicas (red dots) and possible areas with SLG- $R0^\circ$ only, the simulations with $V_{pp\sigma}^0 = 0.2$ eV (Fig. 3(e)) [63] reproduces the \bar{K}_{0° split band measured in ARPES better than with $V_{pp\sigma}^0 = 0$ (Fig. 3(d)). This is in agreement with structural indications of an interlayer coupling.

Finally, we briefly comment on the mechanism of tBLG growth. Because of the high temperature, hBN- $R0^\circ$ does not stabilize *in spite of* the presence of borazine. Yet, *due to* the presence of the surfactant borazine molecule, the graphene layer which grows at this temperature is forced to adopt a lattice orientation close to $R0^\circ$. This is a self-limiting process, because the graphene layer underneath *is not* any more exposed to borazine and therefore

grows in the orientation defined by the SiC substrate to which it is exposed. We believe that this new preparation method, in which a surfactant enables the growth of a graphene layer in an unusual orientation, will foster new approaches to produce large-scale tBLG, thereby bringing its intriguing properties closer to applications.

F.C.B., C.K. and F.S.T. acknowledge funding by the DFG through the SFB 1083 Structure and Dynamics of Internal Interfaces (project A 12). B.A. received funding from the European Union's Horizon 2020 research and innovation program under the Grant Agreement No. 706538. We thank Diamond Light Source for access to beamline I09 (Proposals No. SI20855 and No. SI20810) that contributed to the results presented here. The research leading to this result has been supported by the project CALIPSOplus under the Grant Agreement No. 730872 from the EU Framework Programme for Research and Innovation HORIZON 2020.

* Y.R.L. and N.S. contributed equally to this work.

† Electronic address: f.bocquet@fz-juelich.de

- [1] K. S. Novoselov, A. K. Geim, S. V. Morozov, D. Jiang, Y. Zhang, S. V. Dubonos, I. V. Grigorieva, and A. A. Firsov, Electric Field Effect in Atomically Thin Carbon Films, *Science* **306**, 666 (2004).
- [2] J. M. B. Lopes dos Santos, N. M. R. Peres, and A. H. Castro Neto, Graphene Bilayer with a Twist: Electronic Structure, *Phys. Rev. Lett.* **99**, 256802 (2007).
- [3] A. V. Rozhkov, A. O. Sboychakov, A. L. Rakhmanov, F. Nori, Electronic properties of graphene-based bilayer systems, *Phys. Rep.* **648**, 1 (2016).
- [4] L. Huder, A. Artaud, T. Le Quang, G. Trambly de Lassardière, A. G. M. Jansen, G. Lapertot, C. Chapelier, and V. T. Renard, Electronic Spectrum of Twisted Graphene Layers under Heterostrain, *Phys. Rev. Lett.* **120**, 156405 (2018).
- [5] G. G. Naumis, S. Barraza-Lopez, M. Oliva-Leyva, and H. Terrones, Electronic and optical properties of strained graphene and other strained 2D materials: a review, *Rep. Prog. Phys.* **80**, 096501 (2017).
- [6] H. Kumar, D. Er, L. Dong, J. Li, and V. B. Shenoy, Elastic Deformations in 2D van der waals Heterostructures and their Impact on Optoelectronic Properties: Predictions from a Multiscale Computational Approach, *Sci. Rep.* **5**, 10872 (2015).
- [7] T. E. Beechem, T. Ohta, B. Diaconescu, and J. T. Robinson, Rotational Disorder in Twisted Bilayer Graphene, *ACS Nano* **8**, 1655 (2014).
- [8] T. Stauber, T. Low, and G. Gómez-Santos, Chiral Response of Twisted Bilayer Graphene, *Phys. Rev. Lett.* **120**, 046801 (2018).
- [9] E. S. Morell, L. Chico, and L. Brey, Twisting dirac fermions: circular dichroism in bilayer graphene, *2D Mater.* **4**, 035015 (2017).
- [10] C.-J. Kim, A. Sánchez-Castillo, Z. Ziegler, Y. Ogawa, C. Noguez, and J. Park, Chiral atomically thin films, *Nat. Nanotech.* **11**, 520 (2016).
- [11] A. O. Sboychakov, A. V. Rozhkov, A. L. Rakhmanov, and F. Nori, Externally Controlled Magnetism and Band Gap in Twisted Bilayer Graphene, *Phys. Rev. Lett.* **120**, 266402 (2018).
- [12] L. A. Gonzalez-Arraga, J. L. Lado, F. Guinea, and P. San-Jose, Electrically Controllable Magnetism in Twisted Bilayer Graphene, *Phys. Rev. Lett.* **119**, 107201 (2017).
- [13] A. V. Rozhkov, A. O. Sboychakov, A. L. Rakhmanov, and F. Nori, Single-electron gap in the spectrum of twisted bilayer graphene, *Phys. Rev. B* **95**, 045119 (2017).
- [14] J.-B. Liu, P.-J. Li, Y.-F. Chen, Z.-G. Wang, F. Qi, J.-R. He, B.-J. Zheng, J.-H. Zhou, W.-L. Zhang, L. Gu, and Y.-R. Li, Observation of tunable electrical bandgap in large-area twisted bilayer graphene synthesized by chemical vapor deposition, *Sci. Rep.* **5**, 15285 (2015).
- [15] A. R. Muniz and D. Maroudas, Opening and tuning of band gap by the formation of diamond superlattices in twisted bilayer graphene, *Phys. Rev. B* **86**, 075404 (2012).
- [16] Y. Cao, V. Fatemi, S. Fang, K. Watanabe, T. Taniguchi, E. Kaxiras, and P. Jarillo-Herrero, Unconventional superconductivity in magic-angle graphene superlattices, *Nature* **556**, 43 (2018).
- [17] Y. Cao, V. Fatemi, A. Demir, S. Fang, S. L. Tomarken, J. Y. Luo, J. D. Sanchez-Yamagishi, K. Watanabe, T. Taniguchi, E. Kaxiras, R. C. Ashoori, and P. Jarillo-Herrero, Correlated insulator behaviour at half-filling in magic-angle graphene superlattices, *Nature* **556**, 80 (2018).
- [18] R. Frisenda, E. Navarro-Moratalla, P. Gant, D. Pérez De Lara, P. Jarillo-Herrero, R. V. Gorbachev, and A. Castellanos-Gómez, Recent progress in the assembly of nanodevices and van der Waals heterostructures by deterministic placement of 2D materials, *Chem. Soc. Rev.* **47**, 53 (2018).
- [19] W. Yao, E. Wang, C. Bao, Y. Zhang, K. Zhang, K. Bao, C. K. Chan, C. Chen, J. Avila, M. C. Asensio, J. Zhu, and S. Zhou, Quasicrystalline 30° twisted bilayer graphene as an incommensurate superlattice with strong interlayer coupling, *PNAS* **115**, 6928 (2018).
- [20] W.-J. Zuo, J. B. Qiao, D. L. Ma, L.-J. Yin, G. Sun, J.-Y. Zhang, L.-Y. Guan, and L. He, Scanning tunneling microscopy and spectroscopy of twisted trilayer graphene, *Phys. Rev. B* **97**, 035440 (2018).
- [21] Y. Murata, S. Nie, A. Ebnonnasir, E. Starodub, B. B. Kappes, K. F. McCarty, C. V. Ciobanu, and S. Kondabaka, Growth structure and work function of bilayer graphene on Pd(111), *Phys. Rev. B* **85**, 205443 (2012).
- [22] H. Peng, N. B. M. Schröter, J. Yin, H. Wang, T.-F. Chung, H. Yang, S. Ekahana, Z. Liu, J. Jiang, L. Yang, T. Zhang, C. Chen, H. Ni, A. Barinov, Y. P. Chen, Z. Liu, H. Peng, and Y. Chen, Substrate Doping Effect and Unusually Large Angle van Hove Singularity Evolution in Twisted Bi- and Multilayer Graphene, *Adv. Mat.* **29**, 1606741 (2017).
- [23] F. Hu, S. R. Das, Y. Luan, T.-F. Chung, Y. P. Chen, and Z. Fei, Real-Space Imaging of the Tailored Plasmons in Twisted Bilayer Graphene, *Phys. Rev. Lett.* **119**, 247402 (2017).
- [24] C.-C. Lu, Y.-C. Lin, Z. Liu, C.-H. Yeh, K. Suenaga, and P.-W. Chiu, Twisting Bilayer Graphene Superlattices, *ACS Nano* **7**, 2587 (2013).
- [25] Z. Gao, Q. Zhang, C. H. Naylor, Y. Kim, I. H. Abidi,

J. Ping, P. Ducos, J. Zauberman, M.-Q. Zhao, A. M. Rappe, Z. Luo, L. Ren, and A. T. C. Johnson, Crystalline Bilayer Graphene with Preferential Stacking from Ni–Cu Gradient Alloy, *ACS Nano* **12**, 2275 (2018).

[26] S. Nie, A. L. Walter, N. C. Bartelt, E. Starodub, A. Bostwick, E. Rotenberg, and K. F. McCarty, Growth from Below: Graphene Bilayers on Ir(111), *ACS Nano* **5**, 2298 (2011).

[27] T. Iwasaki, A. A. Zakharov, T. Eelbo, M. Waśniowska, R. Wiesendanger, J. H. Smet, and U. Starke, Formation and structural analysis of twisted bilayer graphene on Ni(111) thin films, *Surf. Sci.* **625**, 44 (2014).

[28] D. S. Lee, C. Riedl, T. Beringer, A. H. Castro Neto, K. von Klitzing, U. Starke, and J. H. Smet, Quantum Hall Effect in Twisted Bilayer Graphene, *Phys. Rev. Lett.* **107**, 216602 (2011).

[29] A. Tejeda, A. Taleb-Ibrahimi, W. de Heer, C. Berger, and E. H. Conrad, Electronic structure of epitaxial graphene grown on the C-face of SiC and its relation to the structure, *New J. Phys.* **14**, 125007 (2012).

[30] I. Razado-Colambo, J. Avila, J.-P. Nys, C. Chen, X. Wallart, M.-C. Asensio, and D. Vignaud, NanoARPES of twisted bilayer graphene on SiC: absence of velocity renormalization for small angles, *Sci. Rep.* **6**, 27261 (2016).

[31] J. Yin, H. Wang, H. Peng, Z. Tan, L. Liao, L. Lin, X. Sun, A. L. Koh, Y. Chen, H. Peng, and Z. Liu, Selectively enhanced photocurrent generation in twisted bilayer graphene with van Hove singularity, *Nat. Comm.* **7**, 10699 (2016).

[32] Z. Tan, J. Yin, C. Chen, H. Wang, L. Lin, L. Sun, J. Wu, X. Sun, H. Yang, Y. Chen, H. Peng, and Z. Liu, Building Large-Domain Twisted Bilayer Graphene with van Hove Singularity, *ACS Nano* **10**, 6725 (2016).

[33] K. V. Emtsev, A. Bostwick, K. Horn, J. Jobst, G. L. Kellogg, L. Ley, J. L. McChesney, T. Ohta, S. A. Reshanov, J. Röhrl, E. Rotenberg, A. K. Schmid, D. Waldmann, H. B. Weber, and T. Seyller, Towards wafer-size graphene layers by atmospheric pressure graphitization of silicon carbide, *Nat. Mater.* **8**, 203 (2009).

[34] S. Forti, K. V. Emtsev, C. Coletti, A. A. Zakharov, C. Riedl, and U. Starke, Large-area homogeneous quasifree standing epitaxial graphene on SiC(0001): Electronic and structural characterization, *Phys. Rev. B* **84**, 125449 (2011).

[35] T. Schumann, M. Dubslaff, M. H. Oliveira, Jr., M. Hanke, J. M. J. Lopes, and H. Riechert, Effect of buffer layer coupling on the lattice parameter of epitaxial graphene on SiC(0001), *Phys. Rev. B* **90**, 041403(R) (2014).

[36] H.-C. Shin, Y. Jang, T.-H. Kim, J.-H. Lee, D.-H. Oh, S. J. Ahn, J. H. Lee, Y. Moon, J.-H. Park, S. J. Yoo, C.-Y. Park, D. Whang, C.-W. Yang, and J. R. Ahn, Epitaxial Growth of a Single-Crystal Hybridized Boron Nitride and Graphene Layer on a Wide-Band Gap Semiconductor, *J. Am. Chem. Soc.* **137**, 6897 (2015).

[37] S. J. Ahn, P. Moon, T.-H. Kim, H.-W. Kim, H.-C. Shin, E. H. Kim, H. W. Cha, S.-J. Kahng, P. Kim, M. Koshino, Y.-W. Son, C.-W. Yang, and J. R. Ahn, Dirac electrons in a dodecagonal graphene quasicrystal, *Science* **361**, 782 (2018).

[38] J. Park, W. C. Mitchel, S. Elhamri, L. Grazulis, J. Hoelscher, K. Mahalingam, C. Hwang, S.-K. Mo, and J. Lee, Observation of the intrinsic bandgap behaviour in as-grown epitaxial twisted graphene, *Nat. Comm.* **6**, 5677 (2015).

[39] U. Starke, J. Schardt, J. Bernhardt, M. Franke, and K. Heinz, Stacking Transformation from Hexagonal to Cubic SiC Induced by Surface Reconstruction: A Seed for Heterostructure Growth, *Phys. Rev. Lett.* **82**, 2107 (1999).

[40] J. Schardt, J. Bernhardt, U. Starke, and K. Heinz, Crystallography of the (3×3) surface reconstruction of 3C-SiC(111), 4H-SiC(0001), and 6H-SiC(0001) surfaces retrieved by low-energy electron diffraction, *Phys. Rev. B* **62**, 10335 (2000).

[41] W. Paszkowicz, J. B. Pelka, M. Knapp, T. Szyszko, and S. Podsiadlo, Lattice parameters and anisotropic thermal expansion of hexagonal boron nitride in the 10–297.5 K temperature range, *Appl. Phys. A* **75**, 431 (2002).

[42] S. Yuan, C. Shen, B. Deng, X. Chen, Q. Guo, Y. Ma, A. Abbas, B. Liu, R. Haiges, C. Ott, T. Nilges, K. Watanabe, T. Taniguchi, O. Sinai, D. Naveh, C. Zhou, and F. Xia, Air-Stable Room-Temperature Mid-Infrared Photodetectors Based on hBN/Black Arsenic Phosphorus/hBN Heterostructures, *Nano Lett.* **18**, 3172 (2018).

[43] H. Hattab, A. T. N'Diaye, D. Wall, C. Klein, G. Jnawali, J. Coraux, C. Busse, R. van Gastel, B. Poelsema, T. Michely, F.-J. Meyer zu Heringdorf, and M. Horn-von Hoegen, Interplay of Wrinkles, Strain, and Lattice Parameter in Graphene on Iridium, *Nano Lett.* **12**, 678 (2011).

[44] C. Riedl, U. Starke, J. Bernhardt, M. Franke, and K. Heinz, Structural properties of the graphene-SiC(0001) interface as a key for the preparation of homogeneous large-terrace graphene surfaces, *Phys. Rev. B* **76**, 245406 (2007).

[45] P. Lauffer, K. V. Emtsev, R. Graupner, T. Seyller, L. Ley, S. A. Reshanov, and H. B. Weber, Atomic and electronic structure of few-layer graphene on SiC(0001) studied with scanning tunneling microscopy and spectroscopy, *Phys. Rev. B* **77**, 155426 (2008).

[46] J. Sforzini, L. Nemec, T. Denig, B. Stadtmüller, T.-L. Lee, C. Kumpf, S. Soubatch, U. Starke, P. Rinke, V. Blum, F. C. Bocquet, and F. S. Tautz, Approaching Truly Freestanding Graphene: The Structure of Hydrogen-Intercalated Graphene on 6H-SiC(0001), *Phys. Rev. Lett.* **114**, 106804 (2015).

[47] E. Koren and U. Duerig, Superlubricity in quasicrystalline twisted bilayer graphene, *Phys. Rev. B* **93**, 201404(R) (2016).

[48] S. Y. Zhou, G.-H. Gweon, A. V. Fedorov, P. N. First, W. A. de Heer, D.-H. Lee, F. Guinea, A. H. Castro Neto, and A. Lanzara, Substrate-induced bandgap opening in epitaxial graphene, *Nat. Mater.* **6**, 770 (2007).

[49] B. Amorim, General theoretical description of angle-resolved photoemission spectroscopy of van der Waals structures, *Phys. Rev. B* **97**, 165414 (2018).

[50] A. Bauer, J. Kräußlich, L. Dressler, P. Kuschnerus, J. Wolf, K. Goetz, P. Käckell, J. Furthmüller, and F. Bechstedt, High-precision determination of atomic positions in crystals: The case of 6H- and 4H-SiC, *Phys. Rev. B* **57**, 2647 (1998).

[51] M. Horn-von Hoegen, Growth of semiconductor layers studied by spot profile analysing low energy electron diffraction – Part I, *Zeit. Kristall.* **214**, 591 (1999).

[52] M. Horn-von Hoegen, Growth of semiconductor layers studied by spot profile analysing low energy electron diffraction – Part II, *Zeit. Kristall.* **214**, 684 (1999).

[53] G. Li, A. Luican, J. M. B. Lopes dos Santos, A. H. Castro

Neto, A. Reina, J. Kong, and E. Y. Andrei, Observation of Van Hove singularities in twisted graphene layers, *Nat. Phys.* **6**, 109 (2010).

[54] Q. Yao, R. van Bremen, G. J. Slotman, L. Zhang, S. Haartsen, K. Sotthewes, P. Bampoulis, P. L. de Boeij, A. van Houselt, S. Yuan, and H. J. W. Zandvliet, Spatially resolved electronic structure of twisted graphene, *Phys. Rev. B* **95**, 245116 (2017).

[55] L. M. Malard, J. Nilsson, D. C. Elias, J. C. Brant, F. Plentz, E. S. Alves, A. H. Castro Neto, and M. A. Pimenta, Probing the electronic structure of bilayer graphene by Raman scattering, *Phys. Rev. B* **76**, 201401(R) (2007).

[56] In this Letter, we use the following terminology. hBN stands for hexagonal boron nitride, G for graphene, SLG for single-layer graphene, and tBLG stands for twisted bilayer graphene. The angle β between the reciprocal unit cell vector and the $\bar{\Gamma}\bar{M}$ direction of the SiC substrate is given with the suffix $R\beta$. In other words, $R0^\circ$ corresponds to the $\bar{\Gamma}\bar{M}$ direction of the SiC, and $R30^\circ$ corresponds to the $\bar{\Gamma}\bar{K}$. The twist angle α in tBLG is given as a prefix, e.g., 30° -tBLG.

[57] The used emissivity ϵ value is 0.825. The measured temperature depends on the SiC doping level and wafer thickness. The temperatures at which the $(\sqrt{3} \times \sqrt{3})R30^\circ$ and (3×3) reconstructions form are used to calibrate the temperature.

[58] The surface Brillouin zone has been calibrated with respect to the 6H-SiC lattice with a reference lattice parameter value of (3.08129 ± 0.00004) Å [50].

[59] Note that the instrumental resolution is approximately four times greater. Typically, a resolution-limited transfer width of 2000 Å is expected for a SPA-LEED instrument [51, 52].

[60] It is well known that in the $(6\sqrt{3} \times 6\sqrt{3})R30^\circ$ buffer layer reconstruction, the low-order diffraction spots of the (6×6) sub-pattern are particularly intense [44, 45].

[61] A similar absorption effect has been reported in nano-ARPES on tBLG with various twist angles and substrates [19, 22, 31].

[62] Compared to the calculation performed in Ref. [49], the value of the graphene intralayer nearest-neighbor intralayer hopping was adjusted ($t = 3.11$ eV for G- $R0^\circ$ and 3.08 eV for G- $R30^\circ$) in order to reproduce the energy at which the avoided crossing is observed. This corresponds to a Fermi velocity of 0.998×10^6 m/s. The interlayer coupling parameter $V_{pp\pi}^0$ was set to -2.7 eV, although its precise value is not important, as the interlayer coupling is dominated by $V_{pp\sigma}^0$. Besides t , $V_{pp\pi}^0$, and $V_{pp\sigma}^0$, all other parameters are the same.

[63] For twisted and untwisted AB-stacked bilayer graphene, $V_{pp\sigma}^0$ ranges from 0.24 to 0.30 eV [53–55].